

# LHC diphoton and Z+photon Higgs signals in the Higgs triplet model with $Y=0$

Lei Wang, Xiao-Fang Han

*Department of Physics, Yantai University, Yantai 264005, China*

## Abstract

We study the implications of the LHC diphoton and Z+photon Higgs signals on the Higgs triplet model with  $Y=0$ , which predicts two neutral CP-even Higgs bosons  $h, H$  and a pair of charged Higgs  $H^\pm$ . We discuss three different scenarios: (i) the observed boson is the light Higgs boson  $h$ ; (ii) it is the heavy Higgs boson  $H$ ; (iii) the observed signal is from the almost degenerate  $h$  and  $H$ . We find that the inclusive Higgs diphoton rates in the first two scenarios can be enhanced or suppressed compared to the SM value, which can respectively fit the ATLAS and CMS diphoton data within  $1\sigma$  range. The inclusive  $ZZ^*$  rates are suppressed, which are outside  $1\sigma$  range of ATLAS data and within  $1\sigma$  range of CMS data. Meanwhile, another CP-even Higgs boson production rate can be suppressed enough not to be observed at the collider. For the third scenario, the Higgs diphoton rate is suppressed, which is outside  $1\sigma$  range of ATLAS data, and the  $ZZ^*$  rate equals to SM value approximately. In addition, we find that the two rates of  $h \rightarrow \gamma\gamma$  and  $h \rightarrow Z\gamma$  have the positive correlations for the three scenarios.

PACS numbers: 14.80.Ec, 12.60.Fr, 14.70.Bh

## I. INTRODUCTION

The CMS and ATLAS collaborations have announced the observation of a new boson around 125.5 GeV [1, 2], which is corroborated by the Tevatron search results [3]. The properties of this particle with large experimental uncertainties are consistent with the SM Higgs boson. Among the various signals, the diphoton and  $ZZ^*$  are the cleanest channels of searching for the Higgs boson. The CMS and ATLAS have presented the constraints [4, 5],

$$\begin{aligned} R_{\gamma\gamma} &= 0.77 \pm 0.27, & R_{ZZ^*} &= 0.92 \pm 0.28 \quad (\text{CMS}), \\ R_{\gamma\gamma} &= 1.6 \pm 0.3, & R_{ZZ^*} &= 1.5 \pm 0.4 \quad (\text{ATLAS}). \end{aligned} \tag{1}$$

The CMS collaboration has released their results of the measurement of  $Z\gamma$  and set an upper limit on the ratio  $R_{Z\gamma} < 10$  [6].

The recent Higgs data has been discussed in the SUSY models[7], little Higgs models [8] and the extensions of Higgs field models, such as the two-Higgs-doublet model [9], the Higgs triplet model ( $Y=2$ ) [10], the models with septuplet [11] and color-octet scalar [12]. In this work, we will study the implications of the LHC diphoton and  $Z$ +photon Higgs signals on the Higgs triplet model with  $Y=0$  (HTM0) [13], which predicts two neutral CP-even Higgs bosons  $h, H$  and a pair of charged Higgs  $H^\pm$ . We will discuss three different scenarios: (i) the observed boson is the light Higgs  $h$ , and the heavy Higgs  $H$  is not observed at the LHC; (ii) it is the heavy Higgs  $H$ , and the light Higgs  $h$  is not observed at the LEP; (iii) the observed signal is from the almost degenerate  $h$  and  $H$ . Also we will pay the particular attention to the correlations between  $h \rightarrow Z\gamma$  and  $h \rightarrow \gamma\gamma$ . Since both of the rates are loop-induced by charged particles, they should be closely correlated. Any new physics effects manifested in the diphoton decay should also alter the  $Z\gamma$  decay [14, 15]

Our work is organized as follows. In Sec. II we recapitulate the Higgs triplet model with  $Y=0$ . In Sec. III we discuss the LHC diphoton Higgs signal and the correlations between  $h \rightarrow Z\gamma$  and  $h \rightarrow \gamma\gamma$ . Finally, we give our conclusion in Sec. IV.

## II. HIGGS TRIPLET MODEL WITH $Y=0$

In the HTM0, a real  $SU(2)_L$  triplet scalar field  $\Sigma$  with  $Y = 0$  is added to the SM Lagrangian in addition to the doublet field  $\Phi$ . These fields can be written as

$$\Sigma = \frac{1}{2} \begin{pmatrix} \delta^0 & \sqrt{2}\delta^+ \\ \sqrt{2}\delta^- & -\delta^0 \end{pmatrix}, \quad \Phi = \begin{pmatrix} \phi^+ \\ \phi^0 \end{pmatrix}. \quad (2)$$

The renormalizable scalar potential can be written as [16]

$$V(\Phi, \Sigma) = -\mu^2 \Phi^\dagger \Phi + \lambda_0 (\Phi^\dagger \Phi)^2 - \frac{1}{2} M_\Sigma^2 F + \frac{b_4}{4} F^2 + a_1 \Phi^\dagger \Sigma \Phi + \frac{a_2}{2} \Phi^\dagger \Phi F, \quad (3)$$

where  $F \equiv (\delta^0)^2 + 2\delta^+ \delta^-$  and all the parameters are real. The Higgs doublet and triplet fields can acquire vacuum expectation values

$$\langle \Phi \rangle = \frac{1}{\sqrt{2}} \begin{pmatrix} 0 \\ v_d \end{pmatrix}, \quad \langle \Delta \rangle = \frac{1}{2} \begin{pmatrix} v_t & 0 \\ 0 & -v_t \end{pmatrix} \quad (4)$$

with  $v^2 = v_d^2 + 4v_t^2 \approx (246 \text{ GeV})^2$ .

After the spontaneous symmetry breaking, the Lagrangian of Eq. (3) predicts the four physical Higgs bosons, including two CP-even Higgs bosons  $h, H$  and a pair of charged Higgs  $H^\pm$ . These mass eigenstates are in general mixtures of the doublet and triplet fields. The mass matrixes of neutral and charged Higgs bosons are [16]

$$\mathcal{M}_0^2 = \begin{pmatrix} 2\lambda_0 v_d^2 & -a_1 v_d/2 + a_2 v_d v_t \\ -a_1 v_d/2 + a_2 v_d v_t & 2b_4 v_t^2 + \frac{a_1 v_d^2}{4v_t} \end{pmatrix} \equiv \begin{pmatrix} A & B \\ B & C \end{pmatrix}, \quad \mathcal{M}_\pm^2 = \begin{pmatrix} a_1 v_t & a_1 v_d/2 \\ a_1 v_d/2 & \frac{a_1 v_d^2}{4v_t} \end{pmatrix}. \quad (5)$$

The physical mass eigenstates and the unphysical electroweak eigenstates are related by rotations through two mixing angles  $\theta_0$  and  $\theta_+$ :

$$\begin{pmatrix} h \\ H \end{pmatrix} = \begin{pmatrix} \cos \theta_0 & \sin \theta_0 \\ -\sin \theta_0 & \cos \theta_0 \end{pmatrix} \begin{pmatrix} \phi^0 \\ \delta^0 \end{pmatrix}, \quad (6)$$

$$\begin{pmatrix} H^\pm \\ G^\pm \end{pmatrix} = \begin{pmatrix} -\sin \theta_\pm & \cos \theta_\pm \\ \cos \theta_\pm & \sin \theta_\pm \end{pmatrix} \begin{pmatrix} \phi^\pm \\ \delta^\pm \end{pmatrix}. \quad (7)$$

Where the Goldstone boson  $G^\pm$  is eaten by the gauge bosons.

Since the experimental value of the  $\rho$  parameter is near unity [17],  $4v_t^2/v_d^2$  is required to be much smaller than unity. In our calculation,  $v_t$  is taken as 1 GeV. The mixing angle  $\theta_{\pm}$  is proportional to  $\frac{v_t}{v_d}$ , therefore it is very small. The charged Higgs mass is given as

$$M_{H^{\pm}}^2 = a_1 v_t \left( 1 + \frac{v_d^2}{4v_t^2} \right). \quad (8)$$

The neutral mixing angle  $\theta_0$  is given as

$$\begin{aligned} c_0 \equiv \cos \theta_0 &= \frac{1}{\sqrt{2}} \left( 1 - \frac{A - C}{\sqrt{(A - C)^2 + 4B^2}} \right)^{1/2}, \\ s_0 \equiv \sin \theta_0 &= -\frac{1}{\sqrt{2}} \frac{B}{|B|} \left( 1 + \frac{A - C}{\sqrt{(A - C)^2 + 4B^2}} \right)^{1/2}. \end{aligned} \quad (9)$$

Where

$$c_0 > \frac{1}{\sqrt{2}} \text{ for } C > A, \quad c_0 < \frac{1}{\sqrt{2}} \text{ for } C < A, \quad c_0 \rightarrow \frac{1}{\sqrt{2}} \text{ for } C \rightarrow A. \quad (10)$$

The neutral Higgs boson masses are given as

$$\begin{aligned} m_h^2 &= \frac{1}{2} \left( A + C - \sqrt{(A - C)^2 + 4B^2} \right), \\ m_H^2 &= \frac{1}{2} \left( A + C + \sqrt{(A - C)^2 + 4B^2} \right). \end{aligned} \quad (11)$$

In our calculations, the involved Higgs couplings are listed as [16]

$$\begin{aligned} h f \bar{f} &: -i \frac{m_f}{v_d} c_0, & H f \bar{f} &: i \frac{m_f}{v_d} s_0, \\ ZZ h &: \frac{2im_Z^2}{v_d} c_0 g^{\mu\nu}, & ZZ H &: -\frac{2im_Z^2}{v_d} s_0 g^{\mu\nu}, \\ W^+ W^- h &: ig_2^2 \left( \frac{1}{2} v_d c_0 + 2v_t s_0 \right) g^{\mu\nu}, & W^+ W^- H &: ig_2^2 \left( -\frac{1}{2} v_d s_0 + 2v_t c_0 \right) g^{\mu\nu}, \\ \gamma H^+ H^- &: ie (p' - p)^\mu, & Z H^+ H^- &: i \left( g_2 c_W - \frac{m_Z}{v_d} s_+^2 \right) (p' - p)^\mu, \\ H^+ H^- h &: -i \left( a_1 c_+ s_+ c_0 - \frac{1}{2} a_1 s_+^2 s_0 + a_2 v_d c_+^2 c_0 + a_2 v_t s_+^2 s_0 + 2b_4 v_t c_+^2 s_0 + 2\lambda_0 v_d s_+^2 c_0 \right), \\ H^+ H^- H &: -i \left( -a_1 c_+ s_+ s_0 - \frac{1}{2} a_1 s_+^2 c_0 - a_2 v_d c_+^2 s_0 + a_2 v_t s_+^2 c_0 + 2b_4 v_t c_+^2 c_0 - 2\lambda_0 v_d s_+^2 s_0 \right). \end{aligned} \quad (12)$$

Where  $s_+ = \sin \theta_+$  and  $c_+ = \cos \theta_+$ . All the momenta flow into the vertex.

### III. THE HIGGS DIPHOTON AND $Z\gamma$ RATES AT THE LHC

In our calculations, we take  $m_h, m_H, a_2, b_4$  and  $v_d, v_t$  as the input parameters, which can determine the values of  $\lambda_0, a_1, m_{H^\pm}$ . As mentioned above,  $v_t$  is taken as 1 GeV. The perturbativity can give the strong constraints on  $a_2$  and  $b_4$ ,

$$-2\sqrt{\pi} \leq a_2 \leq 2\sqrt{\pi}, \quad -2\sqrt{\pi} \leq b_4 \leq 2\sqrt{\pi}. \quad (13)$$

The electroweak  $T$  parameter can give the constraints on the splitting of  $m_H$  and  $m_{H^\pm}$ ,  $(m_H - m_{H^\pm})^2 < 0.96 m_W^2$  [16]. Since the coupling  $H^\pm \bar{f}_i f_j$  is sizably suppressed by  $s_+$ , the search experiments through the top quark decay hardly give the constraints on  $H^\pm$ . The experimental data at the LEP gives the lower bound of the charged Higgs mass,  $m_{H^\pm} > 79.3$  GeV [18].

We discuss three different scenarios: (I) the observed boson is the light Higgs  $h$ ,  $m_h = 125.5$  GeV and  $135 \text{ GeV} \leq m_H \leq 500 \text{ GeV}$ ; (II) it is the heavy Higgs  $H$ ,  $m_H = 125.5$  GeV and  $80 \text{ GeV} \leq m_h \leq 110 \text{ GeV}$ ; (III) the observed signal is from the almost degenerate  $h$  and  $H$ ,  $m_h \simeq m_H \simeq 125.5$  GeV.

As shown in the Eq. (12), the  $h$  couplings to  $f\bar{f}$  and  $WW$  are proportional to  $c_0$  while these couplings of  $H$  are proportional to  $s_0$ . Due to  $v_t \ll v_d$  and  $s_+ \rightarrow 0$ , the  $h$  couplings to  $WW$  and  $H^+H^-$  are sensitive to  $c_0$  while these couplings of  $H$  are sensitive to  $s_0$ . Therefore, the cross sections and the decay widths of  $h(H)$  normalized to SM values can be given as

$$\begin{aligned} \frac{\sigma(gg \rightarrow h(H))}{\sigma_{SM}(gg \rightarrow h(H))} &\simeq \frac{\sigma(pp \rightarrow jjh(H))}{\sigma_{SM}(pp \rightarrow jjh(H))} \\ &\simeq \frac{\sigma(pp \rightarrow Vh(H))}{\sigma_{SM}(pp \rightarrow Vh(H))} \simeq \frac{\sigma(pp \rightarrow h(H)t\bar{t})}{\sigma_{SM}(pp \rightarrow h(H)t\bar{t})} \simeq c_0^2(s_0^2), \\ \frac{\Gamma(h(H) \rightarrow f\bar{f})}{\Gamma_{SM}(h(H) \rightarrow f\bar{f})} &\simeq \frac{\Gamma(h(H) \rightarrow VV)}{\Gamma_{SM}(h(H) \rightarrow VV)} \simeq \frac{\Gamma(h(H) \rightarrow gg)}{\Gamma_{SM}(h(H) \rightarrow gg)} \simeq c_0^2(s_0^2), \end{aligned} \quad (14)$$

where  $V$  denotes  $W, Z$ . Compared to SM, in addition to the modified  $ht\bar{t}$  and  $hWW$  couplings, the charged Higgs  $H^\pm$  will alter the decays  $h \rightarrow \gamma\gamma$  and  $h \rightarrow Z\gamma$  via the one-loop. The corresponding expressions are given in the Appendix A.

The Higgs boson  $\gamma\gamma, ZZ^*$  and  $Z\gamma$  rates of HTM0 normalized to the SM values are

respectively defined as

$$\begin{aligned}
R_{h(H)}(\gamma\gamma) &= \frac{\sigma(pp \rightarrow h(H))}{\sigma_{SM}(pp \rightarrow h(H))} \frac{Br(h(H) \rightarrow \gamma\gamma)}{Br_{SM}(h(H) \rightarrow \gamma\gamma)} \\
&\simeq c_0^2(s_0^2) \frac{\Gamma(h(H) \rightarrow \gamma\gamma)}{c_0^2(s_0^2)\Gamma_{SM}(h(H))} \frac{\Gamma_{SM}(h(H))}{\Gamma_{SM}(h(H) \rightarrow \gamma\gamma)} \simeq \frac{\Gamma(h(H) \rightarrow \gamma\gamma)}{\Gamma_{SM}(h(H) \rightarrow \gamma\gamma)}, \\
R_{h(H)}(ZZ^*) &= \frac{\sigma(pp \rightarrow h(H))}{\sigma_{SM}(pp \rightarrow h(H))} \frac{Br(h(H) \rightarrow ZZ^*)}{Br_{SM}(h(H) \rightarrow ZZ^*)} \\
&\simeq c_0^2(s_0^2) \frac{c_0^2(s_0^2)\Gamma_{SM}(h(H) \rightarrow ZZ^*)}{c_0^2(s_0^2)\Gamma_{SM}(h(H))} \frac{\Gamma_{SM}(h(H))}{\Gamma_{SM}(h(H) \rightarrow ZZ^*)} \simeq c_0^2(s_0^2), \\
R_{h(H)}(Z\gamma) &= \frac{\sigma(pp \rightarrow h(H))}{\sigma_{SM}(pp \rightarrow h(H))} \frac{Br(h(H) \rightarrow Z\gamma)}{Br_{SM}(h(H) \rightarrow Z\gamma)} \\
&\simeq c_0^2(s_0^2) \frac{\Gamma(h(H) \rightarrow Z\gamma)}{c_0^2(s_0^2)\Gamma_{SM}(h(H))} \frac{\Gamma_{SM}(h(H))}{\Gamma_{SM}(h(H) \rightarrow Z\gamma)} \simeq \frac{\Gamma(h(H) \rightarrow Z\gamma)}{\Gamma_{SM}(h(H) \rightarrow Z\gamma)} \quad (15)
\end{aligned}$$

Where  $\sigma(pp \rightarrow h(H))$  is the total cross section of Higgs boson. The analytic expressions in Eq. (14) and Eq. (15) may help us understand the Higgs production and decay well. In our numerical calculations, we take code Hdecay to consider the relevant higher order QCD and electroweak corrections [19].

### A. Scenario I

For the scenario I, the light Higgs  $h$  is the observed boson. Since the observed  $ZZ^*$  rate is consistent with the SM value,  $c_0$  can not be too small. Also, it is important to make sure that the production rate of  $H$  is small enough not to be detected at the LHC. Thus, to obtain a large  $c_0$  and a small  $s_0$ , we require  $C > A$  (see Eq. (10)).

In Fig. 1, we plot  $R_h(\gamma\gamma)$  versus  $a_2$  and  $R_h(\gamma\gamma)$  versus  $m_{H^\pm}$ , respectively. The  $h$  coupling to  $H^+H^-$  is sensitive to the parameter  $a_2$ , which gives the additional contributions to the decay  $h \rightarrow \gamma\gamma$  via one-loop. Fig. 1 shows that the  $H^\pm$  contributions to  $R_h(\gamma\gamma)$  can interfere constructively with  $W$  contributions for  $a_2 < 0$  and interfere destructively for  $a_2 > 0$ , leading  $R_h(\gamma\gamma) > 1$  and  $R_h(\gamma\gamma) < 1$ , which are respectively favored by the enhanced ATLAS diphoton data and the suppressed CMS data. The magnitude becomes sizable as the increasing of the absolute value of  $a_2$  and the decreasing of  $m_{H^\pm}$ .

In Fig. 2, the samples with  $R_h(\gamma\gamma)$  being within  $1\sigma$  range of ATLAS and CMS diphoton data are projected on the plane of  $a_2$  and  $m_{H^\pm}$ . The left panel shows that the  $1\sigma$  ATLAS diphoton data favors  $-3.6 < a_2 < -1.8$  and  $m_{H^\pm} < 190$  GeV. While the CMS data favors  $a_2 > 0$  and allow  $a_2$  to be smaller than 0 for enough large  $m_{H^\pm}$ . The left panel shows that,

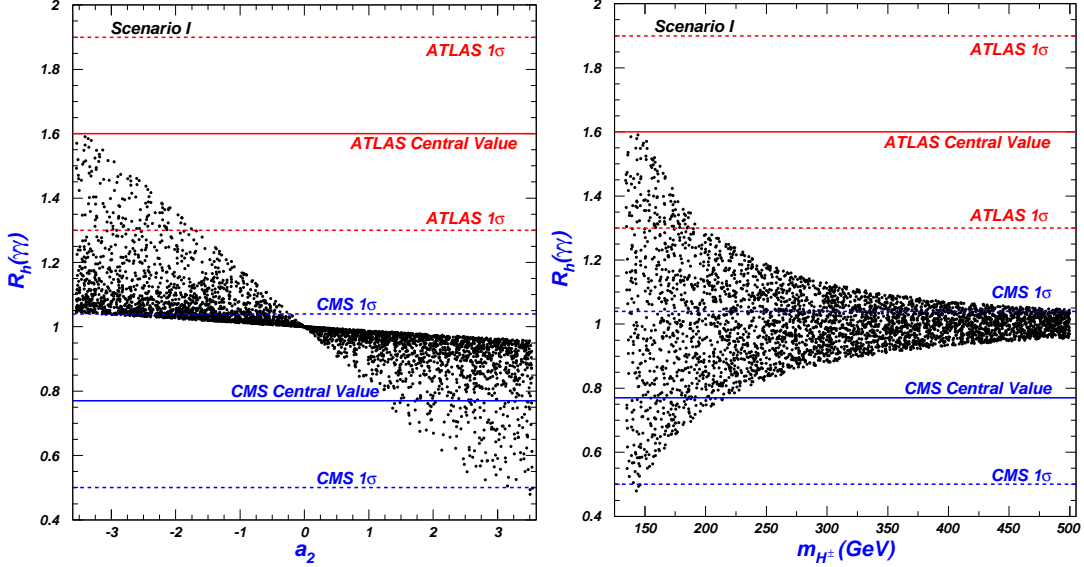


FIG. 1: The scatter plots of the parameter space projected on the planes of  $R_h(\gamma\gamma)$  versus  $a_2$  and  $R_h(\gamma\gamma)$  versus  $m_{H^\pm}$ , respectively.

for  $R_h(\gamma\gamma)$  is within  $1\sigma$  range of ATLAS diphoton data, the samples lie in the region of  $c_0^2 > 0.86$ , and the vast majority of them congregate the region of  $c_0^2 > 0.96$ . The large  $m_{H^\pm}$  favors a large  $c_0^2$ . From the right panel, the value of  $c_0^2$  is larger than 0.98 for  $R_h(\gamma\gamma)$  is within  $1\sigma$  range of CMS diphoton data. Due to  $R_h(ZZ^*) \simeq c_0^2$  (see Eq. 15), the inclusive  $ZZ^*$  rate is outside  $1\sigma$  range of ATLAS data ( $1.5 \pm 0.4$ ), but within  $1\sigma$  range of CMS data ( $0.92 \pm 0.28$ ). Besides, for such large  $c_0^2$ , the corresponding  $s_0^2$  is smaller than 0.14, which will suppress the production rates of  $H$  at the LHC sizably (see Eqs. (14) and (15)), leading that  $H$  is not detected at the LHC.

Fig. 3 shows  $R_h(\gamma\gamma)$  versus  $R_h(Z\gamma)$ . We find that the two rates are positively correlated, and the behavior of  $R_h(Z\gamma)$  is similar to that of  $R_h(\gamma\gamma)$ . Further, the prediction of  $R_h(Z\gamma)$  equals to that of  $R_h(\gamma\gamma)$  approximately.

## B. Scenario II

For the scenario II, the heavy Higgs  $H$  is the observed boson. The parameter  $s_0$  can not be very small to make the observed  $ZZ^*$  rate to be consistent with the experimental data. Besides, it is important to make sure that the production rate of  $h$  is small enough not to be detected at the LEP. Thus, we require  $C < A$  to obtain a large  $s_0$  and a small  $c_0$ , (see

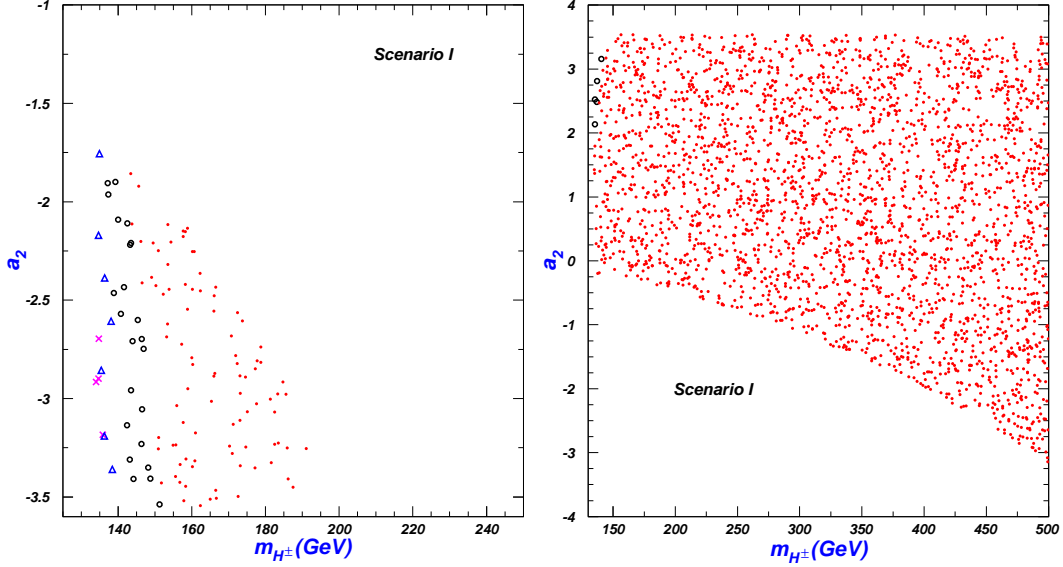


FIG. 2: The scatter plots projected on the plane of  $a_2$  versus  $m_{H^\pm}$ . For the left panel,  $R_h(\gamma\gamma)$  is within  $1\sigma$  range of ATLAS data.  $0.86 < c_0^2 < 0.90$  for the crosses (pink),  $0.90 \leq c_0^2 < 0.95$  for the triangles (blue),  $0.95 \leq c_0^2 < 0.98$  for the circles (black), and  $0.98 \leq c_0^2 < 1.0$  for the bullets (red). The right panel is the same as the left panel, but  $R_h(\gamma\gamma)$  is within  $1\sigma$  range of CMS data.

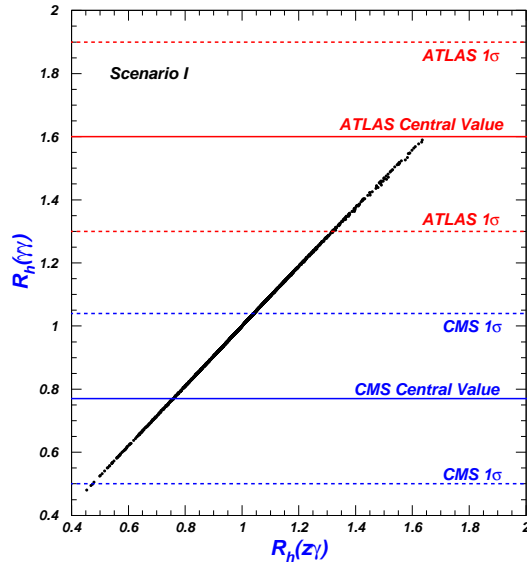


FIG. 3: The scatter plots of the parameter space projected on the plane of  $R_h(\gamma\gamma)$  versus  $R_h(Z\gamma)$ .

Eq. (10)).

In Fig. 4, we plot  $R_H(\gamma\gamma)$  versus  $a_2$  and  $R_H(\gamma\gamma)$  versus  $m_{H^\pm}$ , respectively. Similar to  $R_h(\gamma\gamma)$ ,  $R_H(\gamma\gamma)$  is also larger than 1.0 for  $a_2 < 0$  and smaller than 1.0 for  $a_2 > 0$ .  $R_H(\gamma\gamma)$  can reach 5.0 for  $a_2 \sim -3.5$  and  $m_{H^\pm} \sim 80$  GeV, which is much larger than  $R_h(\gamma\gamma)$  since

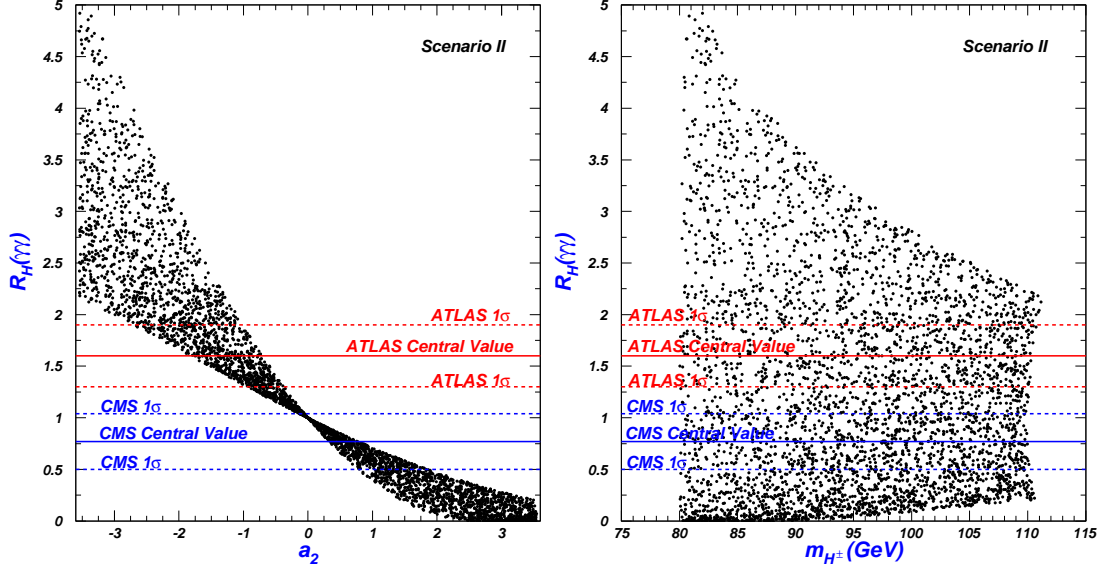


FIG. 4: Same as Fig. 1, but for  $R_H(\gamma\gamma)$ .

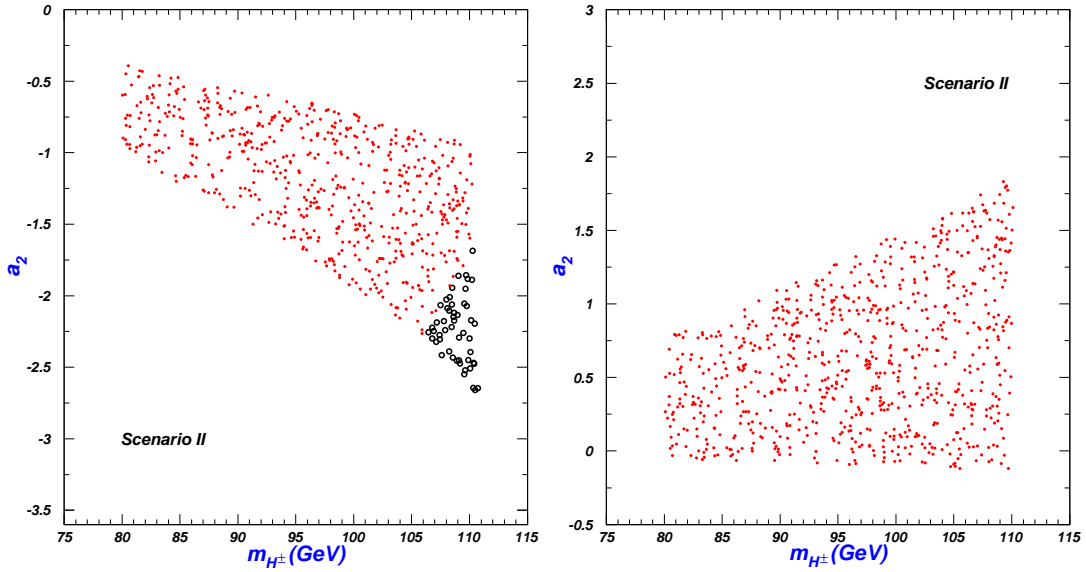


FIG. 5: The Scatter plots projected on the plane of  $a_2$  versus  $m_{H^\pm}$ . For the left panel,  $R_H(\gamma\gamma)$  is within  $1\sigma$  range of ATLAS data.  $0.95 \leq s_0^2 < 0.98$  for the circles (black), and  $0.98 \leq s_0^2 < 1.0$  for the bullets (red). The right panel is the same as the left panel, but  $R_H(\gamma\gamma)$  is within  $1\sigma$  range of CMS data.

$m_{H^\pm}$  for the former is smaller than that for the latter.

In Fig. 5, the samples with  $R_H(\gamma\gamma)$  being within  $1\sigma$  range of ATLAS and CMS diphoton data are projected on the plane of  $a_2$  and  $m_{H^\pm}$ . Fig. 5 shows that  $-2.7 < a_2 < -0.4$  and  $-0.1 < a_2 < 1.9$  are respectively favored by the  $1\sigma$  ATLAS and CMS data. The left panel

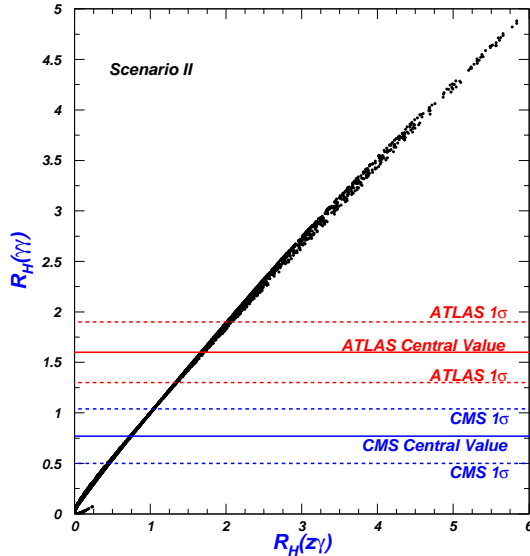


FIG. 6: Same as Fig. 3, but for  $R_H(\gamma\gamma)$  versus  $R_H(Z\gamma)$ .

shows that, for  $R_H(\gamma\gamma)$  is within  $1\sigma$  range of ATLAS diphoton data, the samples lie in the region of  $s_0^2 > 0.95$ , and the vast majority of them congregated in the region of  $s_0^2 > 0.98$ . From the right panel, the value of  $s_0^2$  is larger than 0.98 for  $R_H(\gamma\gamma)$  is within  $1\sigma$  range of CMS diphoton data. The small  $m_{H^\pm}$  favors a large  $s_0^2$ . Due to  $R_H(ZZ^*) \simeq s_0^2$  (see Eq. 15), the inclusive  $ZZ^*$  rate is outside  $1\sigma$  range of ATLAS data, but within  $1\sigma$  range of CMS data. Besides, for such large  $s_0^2$ , the corresponding  $c_0^2$  is smaller than 0.05, and the cross section of  $e^+e^- \rightarrow Zh$  is below the upper limit presented by the LEP [20].

In Fig. 6, we plot  $R_H(\gamma\gamma)$  versus  $R_H(Z\gamma)$ . Similar to scenario I, the two rates are also positively correlated. Especially for the region favored by the  $1\sigma$  range of ATLAS and CMS data, the prediction of  $R_H(Z\gamma)$  equals to that of  $R_H(\gamma\gamma)$  approximately.

### C. Scenario III

For the scenario III, the observed signal is from the almost degenerate  $h$  and  $H$ . We assume that the mass splitting of  $h$  and  $H$  is small enough not to be resolved at current statistics, but large enough so that there is hardly interference between the amplitudes of  $h$  and  $H$ ,  $|m_H - m_h| \gg \Gamma(h), \Gamma(H)$  [21]. Therefore, according to Eq. (11), both the absolute values of  $A - C$  and  $B$  must be very small, but not to equal to zero exactly. For this case, we can obtain a relation of  $m_{H^\pm} \simeq m_h \simeq m_H$  according to Eqs. (5), (8) and (11).

In Fig. 7, we plot  $R_h(\gamma\gamma) + R_H(\gamma\gamma)$  versus  $a_2$  and  $c_0^2$ , respectively. We find that the

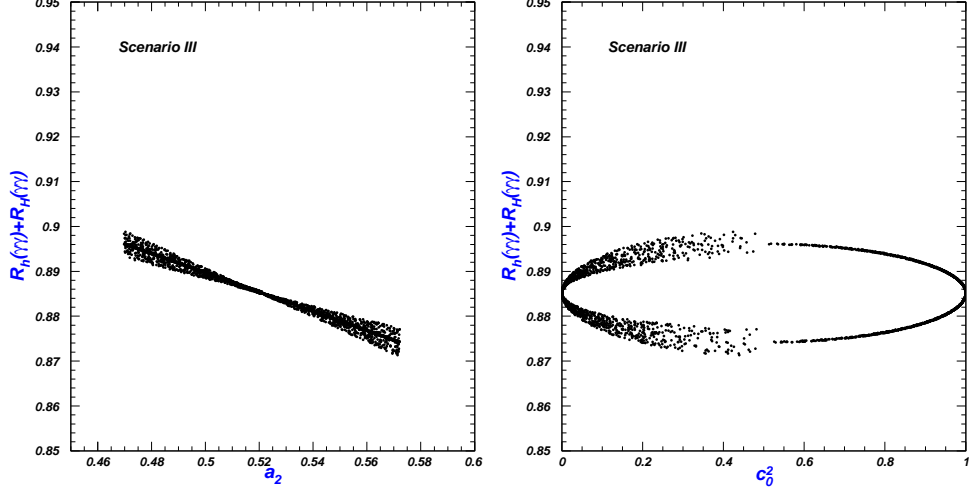


FIG. 7: The scatter plots of the parameter space projected on the planes of  $R_h(\gamma\gamma) + R_H(\gamma\gamma)$  versus  $a_2$  and  $c_0^2$ , respectively.

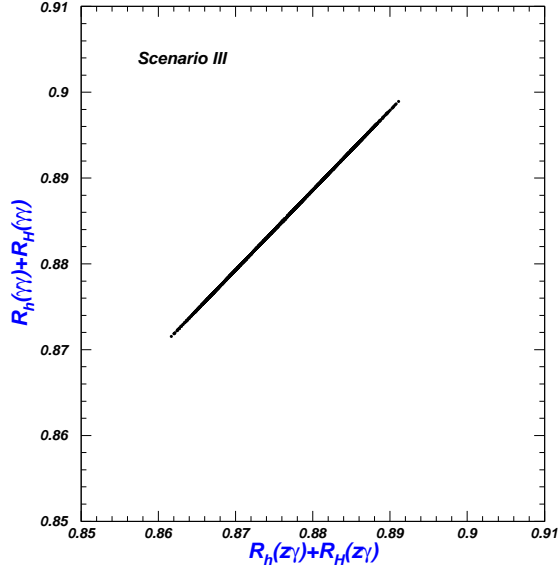


FIG. 8: Same as Fig. 3, but for  $R_h(\gamma\gamma) + R_H(\gamma\gamma)$  versus  $R_h(ZZ^*) + R_H(ZZ^*)$ .

Higgs diphoton rate is suppressed compared to SM value,  $0.87 < R_h(\gamma\gamma) + R_H(\gamma\gamma) < 0.9$ , which is outside  $1\sigma$  range of ATLAS diphoton data, but within  $1\sigma$  range of CMS diphoton data. Due to  $a_1 > 0$ ,  $a_2$  must be larger than zero to obtain a very small  $|B|$  ( $B = -a_1 v_d/2 + a_2 v_d v_t$ ). Thus,  $R_h(\gamma\gamma) + R_H(\gamma\gamma)$  is smaller than 1.0 since the  $H^\pm$  contributions will interfere destructively with the  $W$  contributions for  $a_2 > 0$ . The right panel shows that the large mixing angle  $\theta_0$  may appear. The reason is that  $|A - C|$  still may be much smaller than  $|B|$  although  $|B|$  is very small. Due to  $R_h(ZZ^*) \simeq c_0^2$  and  $R_H(ZZ^*) = s_0^2$  (see Eq. (15)), the inclusive  $ZZ^*$  rate equals to SM prediction value approximately.

In Fig. 8, we plot  $R_h(\gamma\gamma) + R_H(\gamma\gamma)$  versus  $R_h(Z\gamma) + R_H(Z\gamma)$ . We find that the two rates are also positively correlated, and the correlation is more strong than that of scenario II.  $R_h(Z\gamma) + R_H(Z\gamma)$  is allowed to vary in the narrow region,  $0.86 < R_h(Z\gamma) + R_H(Z\gamma) < 0.89$ .

#### IV. CONCLUSION

In the Higgs triplet model with  $Y=0$ , we study the Higgs boson  $\gamma\gamma$  and  $Z\gamma$  rates at the LHC. We studied three different scenarios: (i) the observed boson is the light Higgs boson  $h$ ; (ii) it is the heavy Higgs boson  $H$ ; (iii) the observed signal is from the almost degenerate  $h$  and  $H$ . We found that, for the first two scenarios, the inclusive Higgs diphoton rates can be enhanced or suppressed compared to the SM value, which is respectively within  $1\sigma$  range of ATLAS and CMS data. For the scenario I, the ATLAS data favors  $-3.6 < a_2 < -1.8$  and  $m_{H^\pm} < 190$  GeV. The CMS data favors  $a_2 > 0$  and allow  $a_2$  to be smaller than 0 for enough large  $m_{H^\pm}$ . For the scenario II, the ATLAS and CMS diphoton data favor  $-2.7 < a_2 < -0.4$  and  $-0.1 < a_2 < 1.9$ , respectively. For the first two scenarios, the inclusive  $ZZ^*$  rates are suppressed, which are outside  $1\sigma$  range of ATLAS data and within  $1\sigma$  range of CMS data. For the third scenario, the Higgs diphoton rate is suppressed, which is outside  $1\sigma$  range of ATLAS data, and the  $ZZ^*$  rate equals to SM value approximately. Besides, the two rates of  $h \rightarrow \gamma\gamma$  and  $h \rightarrow Z\gamma$  are positively correlated, and they are approximately equal within the  $1\sigma$  range of ATLAS and CMS diphoton data.

#### Acknowledgment

This work was supported by the National Natural Science Foundation of China (NNSFC) under grant Nos. 11105116, 11005089, and 11175151.

## Appendix A: The expressions for $\Gamma(h \rightarrow \gamma\gamma)$ and $\Gamma(h \rightarrow Z\gamma)$

The charged fermion ( $f$ ), gauge boson ( $W$ ) and scalar ( $s$ ) can contribute to the decay widths of  $h \rightarrow \gamma\gamma$  and  $h \rightarrow Z\gamma$ , which are given by [15, 22]

$$\Gamma(h \rightarrow \gamma\gamma) = \frac{\alpha^2 m_h^3}{256\pi^3 v^2} \left| \sum_f N_f^c Q_f^2 y_f A_{1/2}^{\gamma\gamma}(\tau_f) + y_W A_1^{\gamma\gamma}(\tau_W) + Q_s^2 \frac{v\mu_{hss^*}}{2m_s^2} A_0^{\gamma\gamma}(\tau_s) \right|^2, \quad (\text{A1})$$

$$\begin{aligned} \Gamma(h \rightarrow Z\gamma) &= \frac{\alpha^2 m_h^3}{128\pi^3 s_W^2 c_W^2 v^2} (1 - m_Z^2/m_h^2)^3 \left| N_f^c Q_f y_f \frac{(Q_R^Z + Q_L^Z)}{2} A_{1/2}^{Z\gamma}(\tau_f, \lambda_f) \right. \\ &\quad \left. + Q_W Q_W^Z y_W A_1^{Z\gamma}(\tau_W, \lambda_W) + Q_s Q_s^Z \frac{v g_{hss}}{2m_s^2} A_0^{Z\gamma}(\tau_s, \lambda_s) \right|^2, \end{aligned} \quad (\text{A2})$$

where  $\tau_i = m_h^2/4m_i^2$ ,  $\lambda_i = m_Z^2/4m_i^2$ ,  $Q_W = 1$ ,  $Q_W^Z = c_W^2$ .  $Q_{f,s}$  are the electric charges of fermion and scalar.  $N_f^c$  is the color factor for fermion  $f$ .  $Q_{R,L(s)}^Z = I_{R,L(s)}^3 - Q_{f(s)} s_W^2$  with  $I_{R,L(s)}^3$  being the third isospin components of chiral fermions (scalar).  $y_f$  and  $y_W$  denote the Higgs couplings to  $f\bar{f}$  and  $WW$  normalized to the corresponding SM values.  $g_{hss}$  is the coupling constant of  $hss$ . The loop functions  $A_{(0,1/2,1)}^{\gamma\gamma}$  and  $A_{(0,1/2,1)}^{Z\gamma}$  in Eqs. (A1) and (A2) are defined as

$$\begin{aligned} A_0^{\gamma\gamma}(\tau) &= -[\tau - f(\tau)]\tau^{-2}, \quad A_{1/2}^{\gamma\gamma}(\tau) = 2[\tau + (\tau - 1)f(\tau)]\tau^{-2}, \\ A_1^{\gamma\gamma}(\tau) &= -[2\tau^2 + 3\tau + 3(2\tau - 1)f(\tau)]\tau^{-2}, \\ A_0^{Z\gamma}(\tau, \lambda) &= I_1(\tau, \lambda), \quad A_{1/2}^{Z\gamma}(\tau, \lambda) = -2[I_1(\tau, \lambda) - I_2(\tau, \lambda)], \\ A_1^{Z\gamma}(\tau, \lambda) &= [2(1 + 2\tau)(1 - \lambda) + (1 - 2\tau)]I_1(\tau, \lambda) - 8(1 - \lambda)I_2(\tau, \lambda), \end{aligned} \quad (\text{A3})$$

where

$$\begin{aligned} I_1(\tau, \lambda) &= -\frac{1}{(\tau - \lambda)} + \frac{1}{(\tau - \lambda)^2} [f(\tau) - f(\lambda)] + \frac{2\lambda}{(\tau - \lambda)^2} [g(\tau) - g(\lambda)], \\ I_2(\tau, \lambda) &= \frac{1}{(\tau - \lambda)} [f(\tau) - f(\lambda)], \end{aligned} \quad (\text{A4})$$

with the functions  $f(\tau)$  and  $g(\tau)$  given by

$$f(\tau) = \begin{cases} (\sin^{-1} \sqrt{\tau})^2, & \tau \leq 1 \\ -\frac{1}{4} [\log \frac{1+\sqrt{1-\tau^{-1}}}{1-\sqrt{1-\tau^{-1}}} - i\pi]^2, & \tau > 1 \end{cases}, \quad g(\tau) = \begin{cases} \sqrt{\tau^{-1}-1} (\sin^{-1} \sqrt{\tau}), & \tau \leq 1 \\ \frac{\sqrt{1-\tau^{-1}}}{2} [\log \frac{1+\sqrt{1-\tau^{-1}}}{1-\sqrt{1-\tau^{-1}}} - i\pi], & \tau > 1. \end{cases} \quad (\text{A5})$$

## Appendix B: The vacuum expectation values

The minimization conditions for the tree-level Higgs potential are

$$\left(-\mu^2 + \lambda_0 v_d^2 - \frac{a_1 v_t}{2} + \frac{a_2 v_t^2}{2}\right) v_d = 0, \quad (\text{B1})$$

$$-M_\Sigma^2 v_t + b_4 v_t^3 - \frac{a_1 v_d^2}{4} + \frac{a_2 v_d^2 v_t}{2} = 0. \quad (\text{B2})$$

Solving the Eqs. (B1) and (B2) with **Mathematica**, we can obtain the expressions of  $v_t$  and  $v_d$  in terms of the Lagrangian parameters. However, their expressions are very complicated and lengthy. Therefore, we assume  $v_t$  to be much smaller than 1, and give the approximate solutions for  $a_2 \mu^2 \geq 2M_\Sigma^2 \lambda_0$ ,

$$v_t = \frac{1}{a_1} \left( -\mu^2 + \frac{a_1^2}{4a_2} + \frac{2M_\Sigma^2 \lambda_0}{a_2} + \frac{\sqrt{-128\mu^2 a_2 M_\Sigma^2 \lambda_0 + (a_1^2 + 4\mu^2 a_2 + 8M_\Sigma^2 \lambda_0)^2}}{4a_2} \right), \quad (\text{B3})$$

$$v_d = \sqrt{\frac{M_\Sigma^2}{a_2} + \frac{\mu^2}{2\lambda_0} + \frac{a_1^2}{8a_2 \lambda_0} + \frac{\sqrt{-128\mu^2 a_2 M_\Sigma^2 \lambda_0 + (a_1^2 + 4\mu^2 a_2 + 8M_\Sigma^2 \lambda_0)^2}}{8a_2 \lambda_0}}, \quad (\text{B4})$$

and for  $a_2 \mu^2 \leq 2M_\Sigma^2 \lambda_0$ ,

$$v_t = \frac{1}{a_1} \left( -\mu^2 + \frac{a_1^2}{4a_2} + \frac{2M_\Sigma^2 \lambda_0}{a_2} - \frac{\sqrt{-128\mu^2 a_2 M_\Sigma^2 \lambda_0 + (a_1^2 + 4\mu^2 a_2 + 8M_\Sigma^2 \lambda_0)^2}}{4a_2} \right), \quad (\text{B5})$$

$$v_d = \sqrt{\frac{M_\Sigma^2}{a_2} + \frac{\mu^2}{2\lambda_0} + \frac{a_1^2}{8a_2 \lambda_0} - \frac{\sqrt{-128\mu^2 a_2 M_\Sigma^2 \lambda_0 + (a_1^2 + 4\mu^2 a_2 + 8M_\Sigma^2 \lambda_0)^2}}{8a_2 \lambda_0}}. \quad (\text{B6})$$

From Eqs. (B3) and (B5),  $v_t$  approaches to 0 for  $a_1 \rightarrow 0$ , which is understandable since  $a_1$  is the coefficient of the only term in the Lagrangian breaking the custodial symmetry.

- 
- [1] S. Chatrchyan et al. [CMS Collaboration], Phys. Lett. B **716**, 30 (2012).
  - [2] G. Aad et al. [ATLAS Collaboration], Phys. Lett. B **716**, 1 (2012).
  - [3] T. Aaltonen *et al.* [CDF and D0 Collaborations], Phys. Rev. D **88**, 052014 (2013).
  - [4] [CMS Collaboration], CMS-PAS-HIG-13-005.
  - [5] [ATLAS Collaboration], ATLAS-CONF-2013-034.
  - [6] [CMS Collaboration], CMS-PAS-HIG-12-049.
  - [7] See, e.g., U. Ellwanger, C. Hugonie, Adv. High Energy Phys. **2012**, 625389 (2012); K. Hagiwara, J. S. Lee, J. Nakamura, JHEP **1210**, 002 (2012); N. Christensen, T. Han, S. Su,

- Phys. Rev. D **85**, 115018 (2012); B. Kjae, J.-C. Park, arXiv:1207.3126; J. Cao *et al.*, JHEP **1210**, 079 (2012); JHEP **1203**, 086 (2012); Phys. Lett. B **710**, 665 (2012); H. An, T. Liu, L.-T. Wang, Phys. Rev. D **86**, 075030 (2012); M. Berg, I. Buchberger, D. M. Ghilencea, C. Petersson, arXiv:1212.5009; K. Cheung, C.-T. Lu, T.-C. Yuan, arXiv:1212.1288; T. Liu, L. Wang, J. M. Yang, arXiv:1301.5479; M. Carena, S. Gori, I. Low, N. R. Shah, C. E. M. Wagner, JHEP **1302**, 114 (2013); E. J. Chun, P. Sharma, arXiv:1301.1437; T. Kitahara, T. Yoshinaga, arXiv:1303.0461; Z. Kang, Y. Liu, G. Ning, arXiv:1301.2204; J. Ke, M.-X. Luo, L.-Y. Shan, K. Wang, L. Wang, Phys. Lett. B **718**, 1334 (2013); T. Li, J. A. Maxin, D. V. Nanopoulos, J. W. Walker, Eur. Phys. Jour. C **72**, 2246 (2012); W.-Z. Feng, P. Nath, arXiv:1303.0289; A. Delgado, G. Nardini, M. Quiros, arXiv:1303.0800; T. Kitahara, JHEP **1211**, 021 (2012); K. Schmidt-Hoberg, F. Staub, M. W. Winkler, JHEP **1301**, 124 (2013); K. Benakli, M. D. Goodsell, F. Staub, arXiv:1211.0552.
- [8] L. Wang, J. M. Yang, Phys. Rev. D **84**, 075024 (2011); Phys. Rev. D **79**, 055013 (2009); T. Han, H. E. Logan, B. McElrath, L.-T. Wang, Phys. Lett. B **563**, 191 (2003); C. R. Chen, K. Tobe, C. P. Yuan, Phys. Lett. B **640**, 263 (2006); J. Reuter, M. Tonini, JHEP **1302**, 077 (2013); X.-F. Han, L. Wang, J. M. Yang, J. Zhu, Phys. Rev. D **87**, 055004 (2013); L. Wang, J. M. Yang, J. Zhu, Phys. Rev. D **88**, 075018 (2013).
- [9] See, e.g., C. Haluch, R. Matheus, Phys. Rev. D **85**, 095016 (2012); X.-G. He, B. Ren, J. Tandean, Phys. Rev. D **85**, 093019 (2012); A. Arhrib, R. Benbrik, C.-H. Chen, arXiv:1205.5536; L. Wang, X.-F. Han, JHEP **1205**, 088 (2012); Chang *et al.*, arXiv:1210.3439; N. Chen, H.-J. He, JHEP **1204**, 062 (2012); T. Abe, N. Chen, H.-J. He, JHEP **1301**, 082 (2013); C. Han *et al.*, arXiv:1212.6728; C.-W. Chiang, K. Yagyu, arXiv:1303.0168; R. Jora, S. Nasri, J. Schechter, arXiv:1302.6344; L. Wang, X.-F. Han, arXiv:1312.4759; A. Celis, V. Ilisie, A. Pich, arXiv:1302.4022; W. -F. Chang, J. N. Ng and J. M. S. Wu, Phys. Rev. D **86**, 033003 (2012); M. Chala, JHEP **1301**, 122 (2013).
- [10] A. G. Akeroyd, S. Moretti, Phys. Rev. D **86**, 035015 (2012); A. Arhrib *et al.*, JHEP **1204**, 136 (2012); L. Wang, X.-F. Han, Phys. Rev. D **86**, 095007 (2012); Phys. Rev. D **87**, 015015 (2013); Y. Kajiyama, H. Okada, K. Yagyu, arXiv:1303.3463; P. S. B. Dev, D. K. Ghosh, N. Okada, I. Saha, arXiv:1301.3453; F. Arbabifar, S. Bahrami, M. Frank, Phys. Rev. D **87**, 015020 (2013); C. Englert, E. Re, M. Spannowsky, arXiv:1302.6505; A. Melfo, M. Nemevsek, F. Nesti, G. Senjanovic and Y. Zhang, Phys. Rev. D **85**, 055018 (2012).

- [11] Y. Cai, W. Chao, S. Yang, JHEP **1212**, 043 (2012).
- [12] J. Cao, P. Wan, J. M. Yang, J. Zhu, arXiv:1303.2426.
- [13] D. A. Ross, M. J. G. Veltman, Nucl. Phys. B **95**, 135 (1975); J. F. Gunion, R. Vega and J. Wudka, Phys. Rev. D **42**, 1673 (1990).
- [14] C. Chiang and K. Yagyu, arXiv:1207.1065; P. S. B. Dev et al., arXiv:1301.3453; B. Coleppa, K. Kumar, H. E. Logan, Phys. Rev. D **86**, 075022 (2012); J. Cao, L. Wu, P. Wu, J. M. Yang, arXiv:1301.4641.
- [15] C.-S. Chen, C.-Q. Geng, D. Huang, L.-H. Tsai, arXiv:1302.0502; arXiv:1301.4694.
- [16] P. F. Perez, H. H. Patel, M. J. Ramsey-Musolf, K. Wang, Phys. Rev. D **79**, 055024 (2009).
- [17] S. Kanemura, K. Yagyu, Phys. Rev. D **85**, 115009 (2012).
- [18] ALEPH Collaboration, Phys. Lett. B **543**, 1 (2002); J. Abdallah, et al. [ DELPHI Collaboration], Eur. Phys. Jour. C **34**, 399 (2004).
- [19] A. Djouadj, J. Kalinowski, and M. Spira, Comput. Phys. Commun. **108**, 56 (1998).
- [20] R. Barate et al. [LEP Working Group for Higgs boson searches and ALEPH and DELPHI and L3 and OPAL Collaborations], Phys. Lett. B **565**, 61 (2003); S. Schael et al. [ALEPH and DELPHI and L3 and OPAL and LEP Working Group for Higgs Boson Searches Collaborations], Eur. Phys. Jour. C **47**, 547 (2006).
- [21] B. Batell, D. McKeen, and M. Pospelov, JHEP **1210**, 104 (2012).
- [22] A. Djouadi, Phys. Rept. **459**, 1 (2008).